

Implications of XENON100 results for Dark Matter models and for the LHC

Marco Farina^a, Mario Kadastik^b, Duccio Pappadopulo^c,
Joosep Pata^d, Martti Raidal^b, Alessandro Strumia^{b,e}

(a) *Scuola Normale Superiore and INFN, Piazza dei Cavalieri 7, 56126 Pisa, Italia*

(b) *National Institute of Chemical Physics and Biophysics, Ravala 10, Tallinn, Estonia*

(c) *Institut de Théorie des Phénomènes Physiques, EPFL, CH-1015 Lausanne, Switzerland*

(d) *Department of Physics, University of Tartu, Estonia*

(e) *Dipartimento di Fisica dell'Università di Pisa and INFN, Italia*

Abstract

We perform a fit to the recent XENON100 data and study its implications for Dark Matter scenarios. We find that Inelastic Dark Matter scattering off Na is excluded as an explanation to the DAMA/LIBRA annual modulation signal. Concerning the scalar singlet DM model, we find that the XENON100 data disfavors its constrained limit. We study the CMSSM as well as the low scale phenomenological pMSSM taking into account the recent constraints on supersymmetry from the 2010 LHC run. The global fits are mildly affected as XENON100 disfavors the “well-tempered” bino/higgsino, and the associated “focus-point” region of the CMSSM parameter space. The implications of XENON100 data for Dark Matter annihilation scenarios and for the LHC experiments are outlined.

1 Introduction

The best motivated candidates for the cold Dark Matter (DM) of the Universe [1] are Weakly Interacting Massive Particles (WIMPs) [2]. Indeed, a stable particle with a typical weak interaction cross section of 1 pb and a mass of order 100 GeV naturally produces the observed DM thermal relic abundance. Because the evidence for DM is purely gravitational, there are many particle physics models for WIMPs. Theoretically most appealing ones among those are the DM models based on supersymmetry (SUSY) [3] in which the DM is stable due to the existence of discrete Z_2 symmetry – the R-parity [4] or equivalently the matter parity [5]. Because the matter parity may occur also in the scalar extensions of the standard model (SM) [6], the scalar DM models are also well motivated from the underlying unified physics point of view.

The WIMPs have been searched for in the LEP, Tevatron and LHC experiments as well as in the underground DM direct detection experiments that detect DM recoils on nuclei. The history of DM direct detection experiments can be characterized with their sensitivity to the spin-independent DM-nucleon interaction cross section σ_{SI} as follows.

1. The non-relativistic DM annihilation cross section suggested by the observed cosmological DM abundance is $\sigma \sim 1/(T_0 M_{\text{Pl}}) \approx 3 \cdot 10^{-26} \text{ cm}^3/\text{s} = 10^{-36} \text{ cm}^2$. Such a large value of σ_{SI} is clearly excluded unless the DM particles have peculiar properties or their interactions are restricted to untested sectors.
2. DM that interacts with the Z boson: $\sigma_{\text{SI}} \approx \alpha^2 m_N^2 / M_Z^4 \approx 10^{-38} \text{ cm}^2$. Again, generic WIMPs of this type have been excluded.
3. DM that interacts with the Higgs boson: $\sigma_{\text{SI}} \approx \alpha^2 m_N^4 / M_{\text{DM}}^2 M_Z^4 \approx 10^{-43} \text{ cm}^2$, having assumed that the DM-DM-Higgs coupling is comparable with the weak coupling α .
4. DM that interacts with the W^\pm boson and consequently at loop level with nucleons [7], $\sigma_{\text{SI}} \approx \alpha^4 m_N^4 / (4\pi)^2 M_{\text{DM}}^2 M_W^6 \approx 10^{-46} \text{ cm}^2$, as predicted e.g. by Minimal Dark Matter [8].

Therefore the present most sensitive DM direct search experiments like CDMS [9], EDELWEISS [10] and XENON100 [11] are testing particle physics models in which DM is coupled to the Higgs boson or in which the DM interactions with matter occur only at loop level.

Although the CDMS, EDELWEISS and XENON100 searches for the DM have not given a discovery so far, there is a long-standing claim by DAMA/LIBRA [12] that sees an 8σ evidence for an annual modulation in the nuclear recoil signal of low-mass DM. Recently this claim received some support from the results of CoGeNT experiment [13]. In order to reconcile this result with the negative searches from other experiments, un-orthodox DM scenarios such as Inelastic Dark Matter (iDM) [14, 15] have been put forward. Testing all those scenarios is of utmost importance for understanding the nature of DM.

Recently the XENON100 experiment published new data after 101 days of data taking that probes values of the spin-independent DM/nucleus cross section down to $\sigma_{\text{SI}} \approx 7.0 \times 10^{-45} \text{ cm}^2$ [16]. They observed 3 signal candidate events with the expected background of (1.8 ± 0.6) events. This result leads to the most stringent limit on DM interactions today, and further constrains the best motivated DM models.

In this paper we perform a fit to the new XENON100 data and apply the results to constrain several model dependent as well as model independent scenarios of DM. First, motivated by the DAMA/LIBRA anomaly we study whether the iDM, as an explanation to the observed annual modulation, can survive the new XENON100 results. We find that this is not the case and the DAMA/LIBRA anomaly needs another explanation. After that we study the simplest possible DM model, the scalar singlet model. However, most of our effort goes to the studies of SUSY models. We study the Constrained Minimal Supersymmetric Standard Model (CMSSM) as well as the low energy phenomenological MSSM (pMSSM). In doing that we apply also constraints on SUSY parameter space coming from the LHC run in year 2010 [17, 18]. We find that the XENON100 data stringently constrains the “well-tempered” neutralino scenario [19], and excludes the corresponding “focus-point” parameter region of the CMSSM [20]. Therefore we perform a model independent analysis of that scenario. We derive constraints of new XENON100 data on the CMSSM and pMSSM parameter spaces and study the implications of those to the expected results in the LHC experiments.

The paper is organized as follows. In section 2 we perform the fit of new XENON100 data and apply this to iDM in section 3. In section 4 we study the scalar singlet model. In section 5 we study supersymmetric dark matter. We conclude in section 6.

parameter	range	distribution
v_0 km s ⁻¹	200 - 240	Gaussian: 220 ± 10
v_{esc} km s ⁻¹	498 - 618	see [21]
\mathcal{L}_{eff}	$\pm 2\sigma$	see [16]

Table 1: *The parameters ranges for the XENON100 fits.*

2 Fit of XENON100 data

We perform a fit of the new data released by the XENON100 collaboration [16], taken between January and June 2010, which corresponds (before any cut) to an exposure of 101 days \times 48 kg. XENON100 reports 3 events in the signal region which are consistent with an estimated background of 1.8 ± 0.6 events.

For fixed values of M_{DM} and σ_{SI} , the number of signal events expected in a given direct-detection experiment depends on astrophysical, nuclear and experimental parameters which are more or less well-measured. We build a global χ^2 including these extra parameters as nuisances and marginalize over them at the end.

On the astrophysical side one has to know both the local DM density, ρ_{\odot} , and the DM velocity distribution. In the standard halo model the latter is fixed to be a Maxwellian distribution with a given r.m.s. velocity v_0 , truncated at certain escape velocity v_E :

$$\frac{dN}{d\vec{v}} \equiv f(\vec{v}) \propto e^{-v^2/v_0^2} \theta(v - v_E). \quad (1)$$

The preferred values of the two velocities are $v_0 = 220$ km s⁻¹ and $v_E = 544$ km s⁻¹ [21]. We assume that v_0 has a Gaussian uncertainty of ± 10 km s⁻¹, and we allow for a 2σ variation of it in the fit. We take from [21] the probability distribution of the v_E parameter. The local DM density ρ_{\odot} is kept fixed to 0.3 GeV/cm³ since the effect of its variation is just equivalent to an overall rescaling of σ_{SI} (the quantity really probed by direct detection experiments is their product $\sigma_{\text{SI}}\rho_{\odot}$).

In terms of this set of parameters the differential scattering rate per unit detector mass is

$$\frac{dR}{dE_{\text{nr}}} = N_T \frac{\rho_{\odot}}{M_{\text{DM}}} \int_{|\vec{v}| > v_{\text{min}}} d^3v v f(\vec{v}) \frac{d\sigma_{\text{DM} N}}{dE_{\text{nr}}}, \quad (2)$$

where N_T is the number of nuclei in the target per unit detector mass, M_{DM} is the DM mass and v_{min} is the minimal velocity which allows a nuclear recoil with energy E_{nr} . $\sigma_{\text{DM} N}$ is the nucleus-DM cross section.

We will be interested in spin-independent processes. Nuclear physics enters into the determination of form factors which modulates the cross section according to the momentum transfer:

$$\frac{d\sigma_{\text{DM} N}}{dE_{\text{nr}}} = \frac{m_N \sigma_{\text{SI}} (f_p Z + f_n (A - Z))^2}{2v^2 \mu_n^2 f_n^2} F^2(E_{\text{nr}}). \quad (3)$$

Here m_N is the nucleus mass, μ_n is the nucleon-DM reduced mass, and σ_{SI} is the spin-independent nucleon-DM cross section. We fix our choice of F to the standard Helm form factor [22]. We furthermore assume equal coupling strength to both protons and neutrons: $f_p \approx f_n = 1$.

The last important source of uncertainty comes from the experiment itself. In XENON100 the energy of a recoiling nucleus is inferred from the number of recorded photo-electrons (called

S1 signal) emitted after the prompt relaxation of the excited nucleus. The relation between S1 and the recoil energy is given by

$$S1(E_{\text{nr}}) = 3.6 \text{ PE} \times E_{\text{nr}} \times \mathcal{L}_{\text{eff}}(E_{\text{nr}}). \quad (4)$$

The value of the function \mathcal{L}_{eff} at recoil energies (nuclear) smaller than 5 keV is not measured and must be extrapolated. Such extrapolation is crucial to put limits on light dark matter: the larger \mathcal{L}_{eff} is, the stronger the limits are. We use the recent \mathcal{L}_{eff} measurement from [16], based on [23], and we allow in our fit 2σ excursions from its central value.

In view of the small number of observed events we perform an event-by-event fit, such that we construct the χ -square [24]

$$\hat{\chi}_{\text{Xenon100}}^2(M_{\text{DM}}, \sigma_{\text{SI}}, \{p_i\}) = \hat{\chi}_{\{p_i\}}^2(M_{\text{DM}}, \sigma_{\text{SI}}) + \sum_i \chi_i^2(p_i), \quad (5)$$

where χ_i^2 is the one associated to the parameters themselves and $\hat{\chi}_{\{p_i\}}^2$ is the χ -square for fixed values of the parameters p_i (v_0 , v_{esc} and \mathcal{L}_{eff}), evaluated in terms of the S1 signal along the lines of [11]. We thus include both a Poissonian smearing of the signal and a Gaussian smearing of the energy measurement. The events are collected in the window $3 \text{ PE} \leq S1 \leq 30 \text{ PE}$. We use the acceptance from [16] and we model the background as a flat distribution in the signal region normalized to reproduce the expected number of background events.

We then marginalize $\hat{\chi}_{\text{Xenon100}}^2$ with respect to the nuisance parameters p_i defining

$$\chi_{\text{Xenon100}}^2(M_{\text{DM}}, \sigma_{\text{SI}}) = \min_{\{p_i\}} \hat{\chi}_{\text{Xenon100}}^2(M_{\text{DM}}, \sigma_{\text{SI}}, \{p_i\}), \quad (6)$$

where the minimum is taken in the range summarized in Table 1.

3 Inelastic Dark Matter

The DAMA collaboration reported an 8σ evidence for an annual modulation of their nuclear recoil signal [12] which is compatible with light dark matter scattering on nuclei. Such signal conflicts with other direct detection experiments and (as already remarked by the XENON100 Collaboration [16]) is strongly disfavored by XENON100 under the assumption of an elastic interaction of the dark matter with the Na nuclei of the DAMA detector. We show this in Fig. 1 where we plot the region favored by elastic scattering on sodium at DAMA together with the XENON100 exclusions. The DAMA confidence levels are obtained by a simple χ^2 fit of the first 12 bin of Fig. 9 in [12], showing the measured modulated rate.

The strong bounds already from previous experiments, prompted theorists to consider Inelastic Dark Matter [14] (iDM), namely the idea that the DM detection process could be $\text{DM } N \rightarrow \text{DM}' N$ where the new state DM' is heavier than the DM state by an amount $\delta = M_{\text{DM}'} - M_{\text{DM}}$. It was pointed out that the modified kinematics could make the DAMA anomaly compatible with experiments, such as CDMS, that use lighter nuclei. Indeed the minimum DM velocity needed to scatter on a nucleus with mass m_N giving recoil energy E_{nr} is [14]

$$v_{\text{min}} > \sqrt{\frac{1}{2m_N E_{\text{nr}}}} \left(\frac{m_N E_{\text{nr}}}{\mu_N} + \delta \right), \quad (7)$$

where μ_N is the reduced mass of the DM/nucleus. For the mechanism to be effective the inelasticity mass splitting is assumed to be around 100 keV, which is the order of the typical

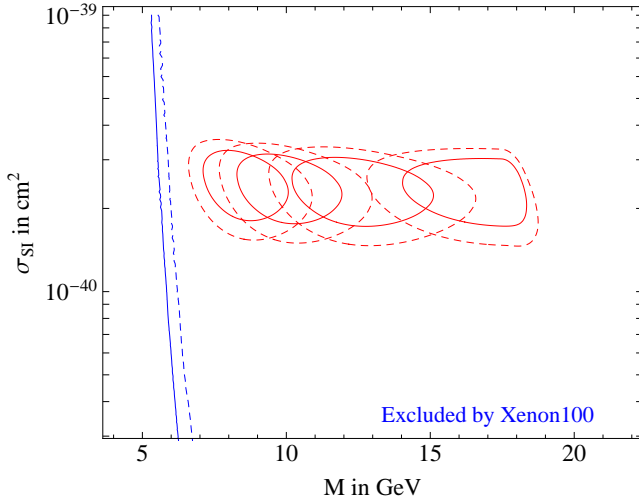


Figure 1: *The 95, 99.7% confidence level contours for 2 d.o.f. for the DAMA modulated signal under the assumption of elastic scattering on sodium atoms. We assume different values of the sodium quenching factor, 0.2, 0.3, 0.4 and 0.5, from right to left. The blue lines are the XENON100 exclusion curves at 95% (continuous curve), 99.7% (dashed) confidence level. We assume $v_0 = 220 \text{ km s}^{-1}$ and $v_{\text{esc}} = 544 \text{ km s}^{-1}$ for the DAMA fit. We neglect channeling.*

nuclear recoil energy. By assuming progressively smaller tails of the uncertain DM velocity it is possible to avoid progressively stronger constraints from experiments with light nuclei. For the same reason it is possible to enhance the relative modulation in the signal claimed by DAMA.

Xenon nuclei have a mass very close to iodine which is, at DAMA, the dominant source of recoils for DM particles with mass above $\mathcal{O}(10 \text{ GeV})$. This fact, together with the high exposure of XENON100 allows to put strong constraints on the iDM hypothesis. This is shown in Fig. 2 where we plot 95% and 99.7% confidence level contours for the parameters favored by DAMA in the $(\delta, \sigma_{\text{SI}})$ plane, together with the XENON100 exclusion curves. The v_0 , v_{esc} and \mathcal{L}_{eff} parameters have been here fixed to their median values. We find that the iDM hypothesis to explain DAMA is excluded throughout its parameter space. This conclusion is sound, independent of the various uncertainties thanks to the similarity between Xe and I nuclei. This can be understood in a simple way [15]. The rate observed by DAMA can be written as

$$\mathcal{B} + \mathcal{S}(1 + a \cos \omega(t - t_0)), \quad (8)$$

where \mathcal{B} is a time-independent unknown background, \mathcal{S} is the mean DM signal and a describe the size of the modulation. $t_0 = 2 \text{ June}$, is where the peak of the modulation observed by DAMA is located. The size $a\mathcal{S}$ of the measured modulation is $\sim 0.02 \text{ counts kg}^{-1} \text{ day}^{-1}$ in the range $2 \text{ keV} \leq E_{\text{nr}} \leq 6 \text{ keV}$. Due to the iodine quenching factor, $q_I \approx 0.085$, this region translates to $23 \text{ keV} \leq E_{\text{nr}} \leq 70 \text{ keV}$ at Xenon. In the region of overlap between the former range and the acceptance window $8.4 - 44.6 \text{ keV}$, the DM scattering rate at Xenon is given by

$$R_{\text{Xenon100}} \sim A \times \epsilon \times \mathcal{S} (1/a + \cos \omega(t - t_0)). \quad (9)$$

ϵ and A are respectively the efficiency of the XENON100 cuts and its acceptance. Together they amounts to roughly 0.2. Integrating eq. (9) over the energy range and over the time of Xenon data-taking one finds

$$N_{\text{Xenon100}} > \mathcal{O}(50) \text{ events}, \quad (10)$$

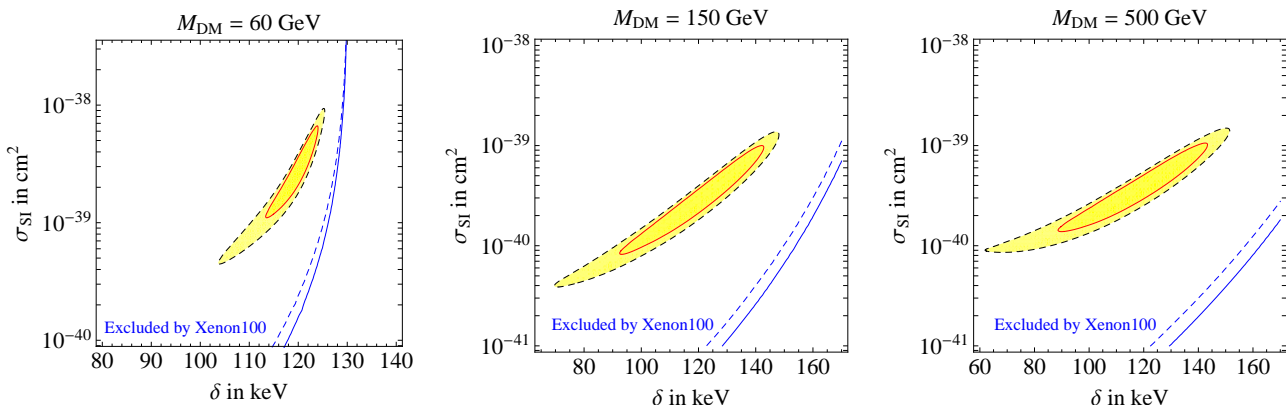


Figure 2: *The 95, 99.7% confidence level contours for 2 d.o.f. for iDM fit to DAMA, together with the 95, 99.7% exclusion curves from XENON100 data (full and dashed respectively). We fix the iodine quenching factor to 0.085. Sodium quenching and channeling are irrelevant for these values of the mass.*

where we folded in the exposure and we used $a < 1$. It is thus clear where the exclusion curves shown in Fig. 2 comes from.

As a final comment, it has been recently proposed that DM scattering at DAMA may not occur on iodine or sodium nuclei, but on thallium impurities [25], present in NaI crystal as a dopant at the $\approx 10^{-3}$ level. Due to the large nuclear size ($A \approx 205$), thallium can be the primary scatterer if δ is big enough to kinematically forbid scattering on iodine, and can explain the DAMA modulation with a large enough $\sigma_{SI} \sim 10^{-34} \text{cm}^2$. These large cross sections avoid other direct-detection searches if scattering at other experiments is kinematically forbidden. Since the nuclear mass of the nuclei in all currently available experiments is smaller than the one of thallium, one can always find values of δ and of M_{DM} where this is realized. This is true for CRESST-II, using tungsten ($A \approx 184$) as a target, and for XENON100 ($A \approx 132$).

4 Scalar singlet Dark Matter model

We consider a DM model obtained adding to the Standard Model a Dark Matter real singlet scalar field S coupled to the Higgs doublet H as described by the following Lagrangian [26, 27, 28, 29]:

$$\mathcal{L} = \mathcal{L}_{SM} + \frac{(\partial_\mu S)^2}{2} - \frac{m^2}{2} S^2 - \lambda S^2 |H|^2, \quad (11)$$

invariant under the matter parity $S \rightarrow -S$, the discrete gauge symmetry of scalars carrying $B - L$ [6]. S is the DM field and its mass is given by $M_{DM}^2 = m^2 + \lambda V^2$ with $V = 246 \text{ GeV}$. So the model has 2 free parameters, M_{DM} and λ . Assuming that the relic DM abundance equals its cosmologically measured value the model is able of predicting the relation in the plane (M_{DM}, σ_{SI}) plotted in Fig. 3. Given that the Higgs boson mass is also presently unknown, we plotted such relation for a few values of the Higgs mass: 115 GeV (green, favored by precision data), 140 GeV (yellow, compatible with precision data), 200 GeV (red, disfavored by precision data); 300 GeV (magenta, strongly disfavored by precision data).

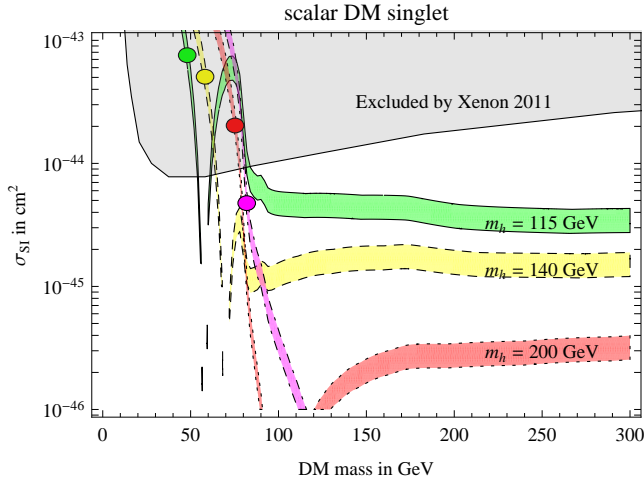


Figure 3: Predictions of the scalar singlet model for a few values of the Higgs boson mass: 115 GeV (green), 140 GeV (yellow), 200 GeV (red), 300 GeV (magenta). The dots are the predictions of the constrained model of [6, 30].

The very small σ_{SI} predicted around $M_{\text{DM}} = m_h/2$ is due to the Higgs resonance enhancement of the cosmological DM annihilation rate. This quantity is computed as in [30], already including the 3 body final states whose relevance was emphasized in [31].

In absence of a theoretical motivation for having m comparable to the Higgs mass, [6, 30] considered the case $m = 0$, such that the model has one parameter less and is able of predicting a point in the plane $(M_{\text{DM}}, \sigma_{\text{SI}})$. Such prediction is also shown in Fig. 3, for the same values of the Higgs boson mass.

We remark two uncertainties not explicit from the plot. First, the XENON100 exclusion bound is plotted assuming $\rho_{\odot} = 0.3 \text{ GeV}/\text{cm}^3$ for the local DM density. This is the canonical value routinely adopted in the literature, with a typical associated error bar of $\pm 0.1 \text{ GeV}/\text{cm}^3$. Recent computations found a higher central value closer to $0.4 \text{ GeV}/\text{cm}^3$ [32] that would imply stronger bounds on the cross section σ_{SI} .

Second, the prediction for the conventional spin-independent DM/nucleon cross section is:

$$\sigma_{\text{SI}} = \frac{\lambda^2 m_N^4 f^2}{\pi M_{\text{DM}}^2 m_h^4}, \quad (12)$$

where f parameterizes the nucleon matrix element:

$$\langle N | m_q \bar{q}q | N \rangle \equiv f_q m_N [\bar{N}N], \quad f = \sum_{q=\{u,d,s,c,b,t\}} f_q = \frac{2}{9} + \frac{5}{9} \sum_{q=\{u,d,s\}} f_q. \quad (13)$$

The main uncertainty comes from f_s . According to recent analyses, $f = 0.56 \pm 0.11$ [33], or $f = 0.30 \pm 0.015$ [34] using lattice results. Here and in the following we assume the default value in the MICROMEAS code: $f = 0.467$ [35].

5 Supersymmetry

In this section we study the impact of new XENON100 data on constraining SUSY models. We first consider the CMSSM, the most popular SUSY model with an unified scalar mass m_0 , an

quantity	experiment	Standard Model
$\alpha_3(M_Z)$ [43]	0.1184 ± 0.0007	parameter
m_t [44]	172.7 ± 1.1	parameter
m_b [45]	4.19 ± 0.12	parameter
$\Omega_{\text{DM}} h^2$ [46]	0.112 ± 0.0056	0
δg_μ [47]	$(2.8 \pm 0.8)10^{-9}$	0
$\text{BR}(B_d \rightarrow X_s \gamma)$ [48]	$(3.50 \pm 0.17) 10^{-4}$	$(3.15 \pm 0.23) 10^{-4}$
$\text{BR}(B_s \rightarrow \mu^+ \mu^-)$ [49]	$(0 \pm 1.4)10^{-8}$	$(0.33 \pm 0.03) 10^{-8}$
$\text{BR}(B_u \rightarrow \tau \bar{\nu})/\text{SM}$ [50]	1.25 ± 0.40	1

Table 2: *The data we fit, together with LHC and XENON100 bounds.*

unified gaugino mass $M_{1/2}$ and an unified trilinear scalar A -term at the GUT scale. Given that XENON100 adds to many other experimental constraints, we perform a global fit to all relevant data as described in the next subsection. Most importantly, we include the recent CMS and ATLAS constraints on the CMSSM parameters space that are based on the LHC 2010 run. Our results agree well with the ones in [36, 37, 38, 39, 40, 41, 42]. As a result we are going to show the complementarity between the XENON100 and LHC results in constraining CMSSM and study the implications of the XENON100 results for the LHC 2011 run.

One of the results of our research is that the “well-tempered” neutralino scenario is stringently constrained by the XENON100 new result. Motivated by that we perform a generic analyses of the “well-tempered” neutralino and show that, quite model independently, this scenario is now stringently constrained.

Finally we relax the CMSSM constraints on the particle spectrum coming from the unification relations and study a generic low energy phenomenological MSSM, the pMSSM. We identify the generic XENON100 constraints on pMSSM.

5.1 Global fit of supersymmetric models

Global fits of the SUSY models have recently been performed by several groups in the context of LHC studies, and our results agree with them. Therefore we focus on the impact of the new XENON100 data in constraining SUSY models. Here, we briefly describe our procedure, and the differences with respect to previous approaches.

We perform a random scan of the parameter space and calculate the sparticle spectrum as well as DM relic abundance using the MICROMEAS public code [35]. We vary the relevant input SM parameters (m_t , α_3 , m_b) within 5σ experimental errors assuming a Gaussian distribution. The CMSSM parameters (m_0 , $M_{1/2}$, A_0 , $\tan\beta$, $\text{sign}(\mu)$) are generated randomly in the ranges $(m_0, M_{1/2}) \sim (0, 4000)$ GeV, $A_0 \sim (-3m_0, 3m_0)$, $\tan\beta \sim (1, 60)$ and $\text{sign}(\mu) = \pm 1$ with a flat distribution. Using MICROMEAS we compute all observables for each sampling point and select those rare cases that reproduce all experimental data within 5σ errors.

We do not use any special technique such as Markov chains, which makes the scanning more efficient, but that might lead to missing some local best-fit regions. Using the computing power of the Baltic Grid we get about 150,000 good points that satisfy all the experimental criteria. For such points we compute the global χ^2 using the data summarized in Table 2,

$$\chi^2 = \chi_{\text{SM parameters}}^2 + \chi_{\text{observables}}^2 + \chi_{\text{LHC}}^2 + \chi_{\text{Xenon100}}^2. \quad (14)$$

Notice that we do not include electroweak precision observables, as the full fit is not well

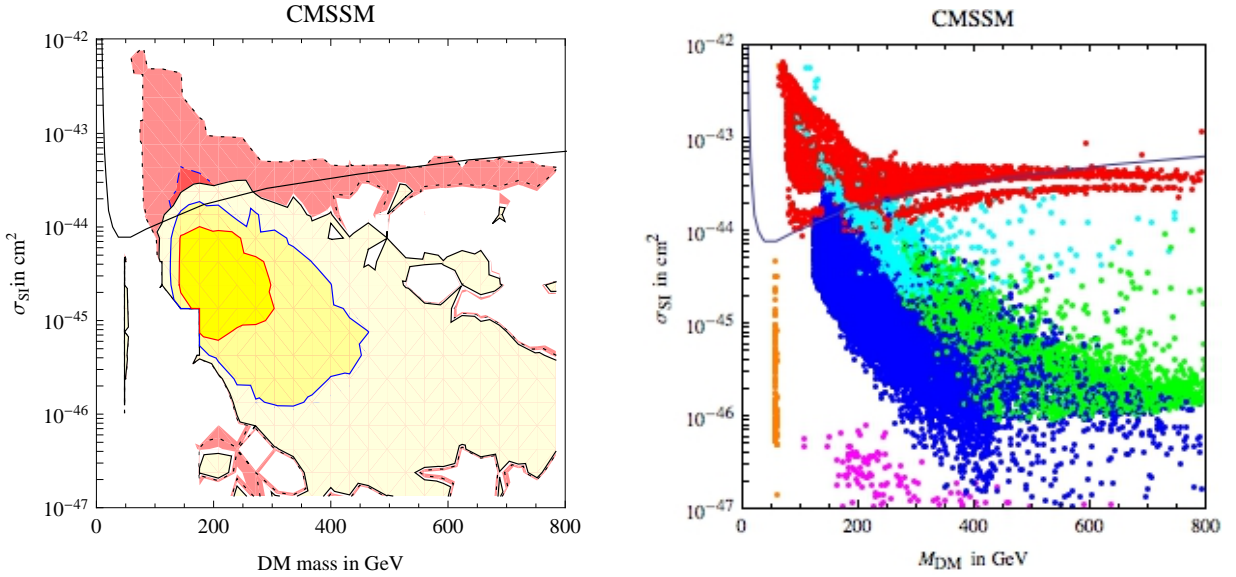


Figure 4: *The $(M_{\text{DM}}, \sigma_{\text{SI}})$ plane in the CMSSM. In the left panel we show the global fit: the yellow regions surrounded by continuous contours are the best fit including the XENON100 and LHC data, at 68, 95, 99.7% confidence levels for 2 d.o.f. The red regions surrounded by dashed contours are the corresponding regions now excluded by XENON100. In the right panel we show points with $\Delta\chi^2 < 4^2$, colored according to the DM annihilation mechanism. The red dots in the upper region excluded by the XENON100 correspond to the “well-tempered” neutralino, orange to the annihilations via light Higgs resonance, green via the heavy Higgs resonance, cyan via neutral Higgses with $\tan\beta$ -enhanced couplings, blue via slepton co-annihilations, magenta via stop co-annihilations.*

approximated simply by the oblique parameters that do not have a significant impact on the result [51].

In this work we perform a purely phenomenological fit, considering values of the sparticles masses significantly above the weak scale (up to 4 TeV), ignoring the theoretical issue of naturalness (see [52, 53] for a recent analysis). Technically, this is achieved as follows: when plotting the χ^2 as function of one or two parameters, we minimize it with respect to all other parameters. The fit is mainly driven by the DM abundance and by the apparent anomaly in the anomalous magnetic moment of the muon, and agrees with the fits in [38, 39, 54]. Given that it might not be a real anomaly, we also show regions at relatively high confidence levels.

We keep the nuclear matrix elements and the DM local density fixed to their default values in MICROMEAS, as already discussed in the previous section. We will comment about the effect of such extra uncertainties.

5.2 The CMSSM results

Fig. 4a shows our global CMSSM fit for the DM mass M_{DM} and spin-independent DM-nucleus cross section σ_{SI} measured by XENON100 experiment. The yellow regions surrounded by continuous contours are the best fit regions including the XENON100 and LHC data, at 1, 2 and 3σ level (68, 95, 99.7% confidence levels for 2 d.o.f). We also show, as red regions surrounded by dashed contours, the previous best-fit regions at the same confidence levels now excluded

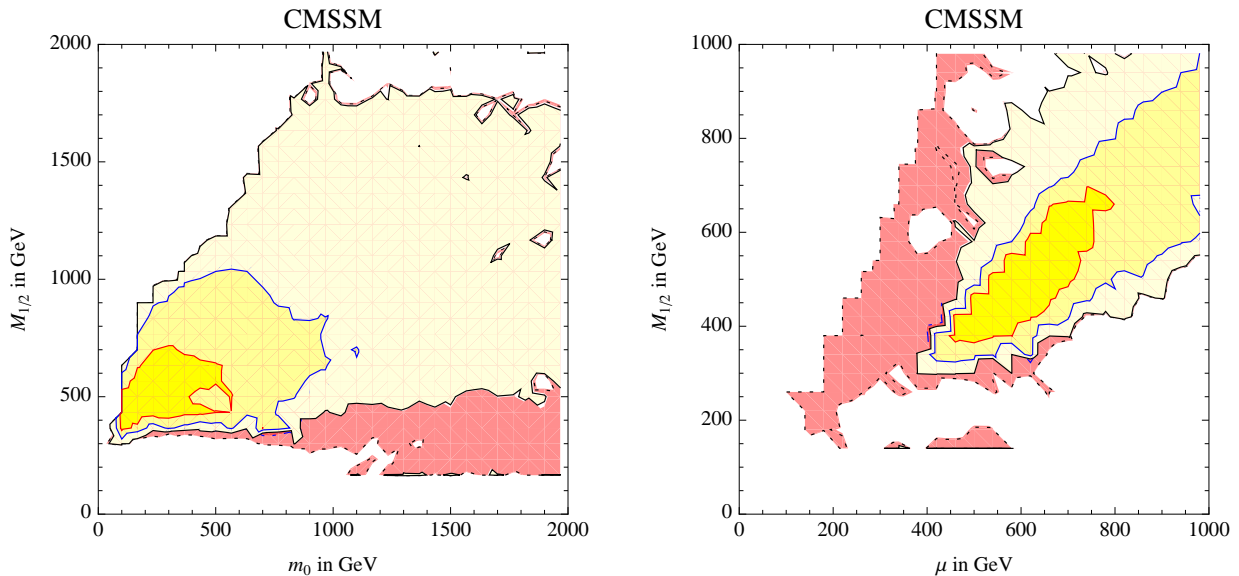


Figure 5: *Global CMSSM fits in $(m_0, M_{1/2})$ (left) and in $(\mu, M_{1/2})$ (right) planes. The red contours are excluded by XENON100, other details are as in Fig. 4a.*

by XENON100 at more than 3σ . Obviously, such excluded regions lie around the XENON100 exclusion bound at 90% confidence level (the continuous curve in the figure).

Within the CMSSM, thermal freeze-out of neutralino DM can reproduce the observed DM cosmological abundance according to a few qualitatively distinct mechanisms, that correspond to different fine-tunings. To interpret this result we therefore discriminate such distinct cases, plotting in Fig. 4b the points of the CMSSM parameter space (also imposing a reasonably good global fit, $\Delta\chi^2 < 4^2$) colored according to their dominant DM annihilation mechanisms. We identify the following distinctive regions:

1. Red points (“arm” in the upper part of the plot) have $|\mu| \approx M_1$ such that the lightest neutralino has a significant Higgsino component (“well-tempered” neutralino [19]). In the CMSSM this happens in the fine-tuned region with large m_0 and small μ in the so-called “focus-point” region [20]. The double structure of the “arm” in Fig. 4b shows that both signs of the μ parameter can give the correct DM relic abundance while $\mu > 0$ is favored by the $(g - 2)_\mu$ anomaly. Comparison with Fig. 4a shows that the new XENON100 data excludes or disfavors this scenario.
2. Blue points (around the center of the plot) have $m_{\tilde{e}} \approx M_{\text{DM}}$, corresponding to slepton co-annihilations. They provide the best global fit.
3. Orange points (around the line at $M_{\text{DM}} \approx m_h/2$) correspond to the Higgs resonance mechanism. This part of the parameter space is allowed by the global fit only at 3σ level.
4. Green points (around the bottom-right part of the figure) have $M_{\text{DM}} \approx m_A/2$, corresponding to the resonant DM annihilations mediated by the CP-odd Higgs boson A .
5. Cyan points represent parameters in which one moves away from Higgs resonances (we arbitrarily assume a 10% off-degeneracy to discriminate from the previous case) but the DM annihilation processes are still mediated via all neutral Higgses in s -channel. A large

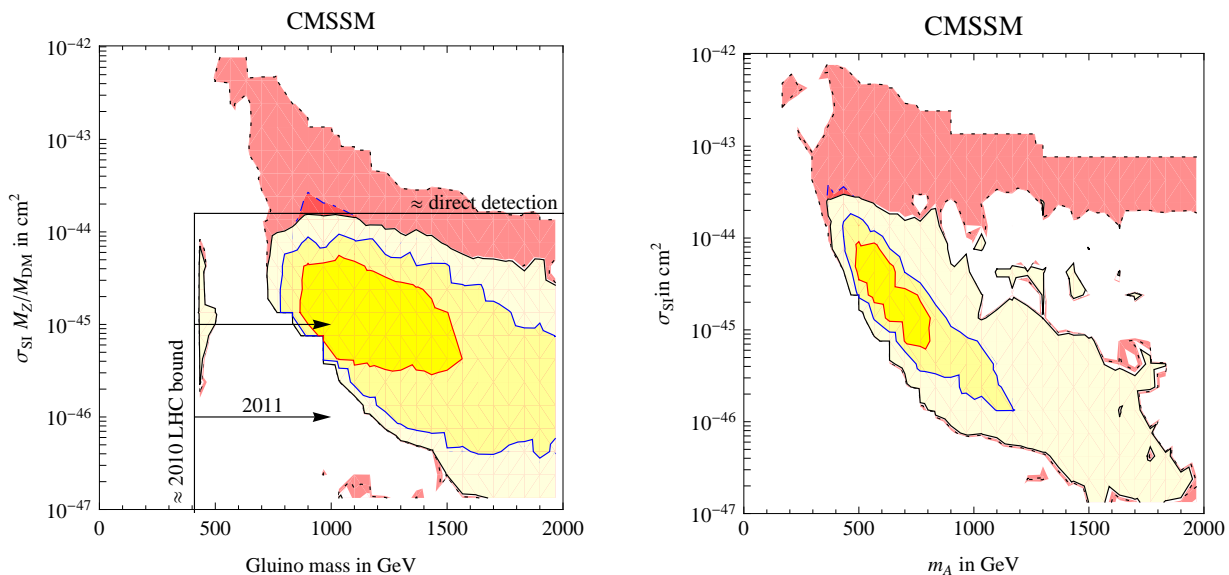


Figure 6: Global CMSSM fits in $(M_{\tilde{g}}, \sigma_{\text{SI}})$ (left) and in $(m_A, \sigma_{\text{SI}})$ (right) planes. The red contours are excluded by XENON100, other details are as in Fig. 4a.

enough Higgs couplings to the SM fermions and to DM is obtained thanks to $\tan \beta > 45$ and to a non-negligible Higgsino component of the DM neutralino. Consequently some of these points have a large direct detection cross section.

6. Magenta points (at very low σ_{SI}) correspond to stop co-annihilations.

We remark that, within the CMSSM, the LEP and LHC bounds have excluded one more mechanism that was considered more plausible because its non-fine-tuned nature: the bino annihilations via light slepton exchange in t -channel. In the light of our results the experimental data favours slepton co-annihilation as the mechanism for generating neutralino thermal relic abundance.

In the light of these considerations, we can now discuss the global CMSSM fits for other parameters. Fig. 5 shows some 2-dimensional fits as indicated in the figure. We see that XENON100 strongly disfavors regions with small $|\mu|$ and partly also with small $M_{1/2}$ (the very small allowed region at 3σ level for small $M_{1/2}$ below the red excluded region corresponds to the Higgs resonance DM annihilation mechanism). Within the CMSSM a small $|\mu|$ can be realized in the “focus-point” scenario that requires a multi-TeV m_0 . Such a region was previously not favored by global fits and is now further disfavored by the XENON100 bound that disfavors a neutralino DM with a significant higgsino component. The fact that small values of $|\mu|$ below 400 GeV are now excluded by XENON100 data is perhaps one of the most important results of our work.

Fig. 6a compares the LHC prospects (here characterized by the approximate gluino mass reach), with the prospects of direct detection experiments (characterized by $\sigma_{\text{SI}} M_{\text{DM}}/M_Z$, which is the only parameter probed by experiments when M_{DM} is much heavier than the target nucleus). We see that LHC can soon probe the already disfavored Higgs resonance region, that within the CMSSM necessarily has a light gluino with mass $M_3 \approx 400$ GeV, and reach the best-fit region. On the other hand, Fig. 6b shows that, after XENON100, there is a clear correlation between the spin-independent DM direct detection cross section and m_A . Although

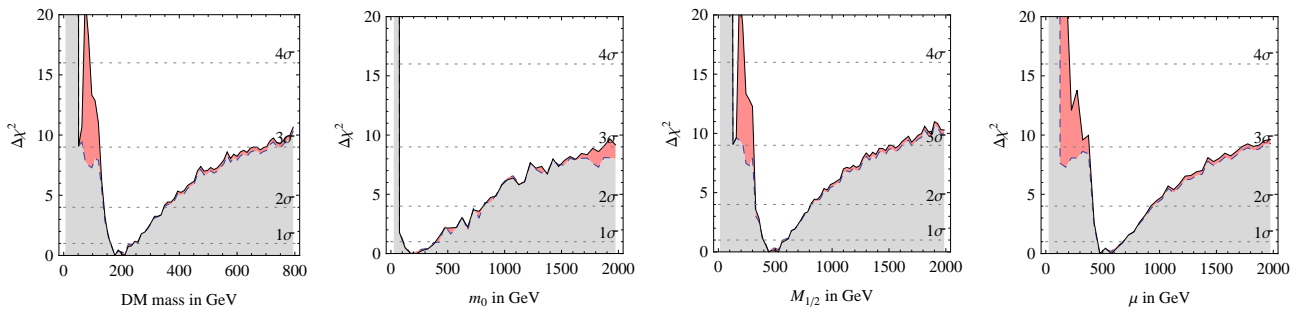


Figure 7: *Global CMSSM fit for the DM mass (left panel) and for the $m_0, M_{1/2}, \mu$ parameters before (dashed curve) and after (continuous curve) including the XENON100 results.*

the XENON100 results exclude only a very small region of the parameter space at low values of m_A , this implies that the CMSSM charged Higgs boson mass must exceed $M_{H^+} > 400$ GeV and is inaccessible at the 7 TeV LHC.

Finally, Fig. 7 shows our fits for the DM mass and for a few key parameters: $m_0, M_{1/2}$ and μ . Within the CMSSM, XENON100 disfavors light M_{DM} (with the exception of the Higgs resonance region at $M_{\text{DM}} \approx m_h/2$). In the light of that result LHC upgrade to the nominal 14 TeV center of mass energy is needed to cover the CMSSM best fit region.

5.3 “Well-tempered” neutralino

As we have shown, within the CMSSM, the XENON100 result has interesting implication on the “well-tempered” neutralino [19]. Here we study this scenario of DM generation in SUSY models in a model-independent way. Within the MSSM, the neutralino is a mixed state of bino, wino, higgsino. None of them, in a pure state, allows thermal DM with a weak scale mass $M_{\text{DM}} \approx M_Z$:

- The pure higgsino couples to the Z too strongly, such that for $M_{\text{DM}} \approx M_Z$ its thermal abundance is too low (the cosmological abundance is obtained for a heavy $M_{\text{DM}} \approx 1$ TeV higgsino); furthermore, for the same reason it is experimentally excluded by direct searches.
- The pure wino similarly has too much co-annihilations with charged winos, such that for $M_{\text{DM}} \approx M_Z$ its thermal abundance is too low (the cosmological abundance is obtained for a heavier $M_{\text{DM}} \approx 2.7$ TeV taking into account electroweak Sommerfeld effects [55]). Contrary to the previous case, having no coupling to the Z it is allowed by direct searches.
- The pure bino, instead, has no couplings and no co-annihilations, such that its cosmological abundance would be too high.

Given that the bino has opposite problems with respect to the higgsino or the wino, it is possible to find a good DM candidate by appropriately mixing them [19]. A mixed bino/wino still has no couplings to the Z , such that it is not interesting for direct detection; furthermore it requires $M_1 \approx M_2$ at the weak scale and is not compatible with unification of gaugino masses, $M_1 \approx M_2 \approx M_3$ at the GUT scale.

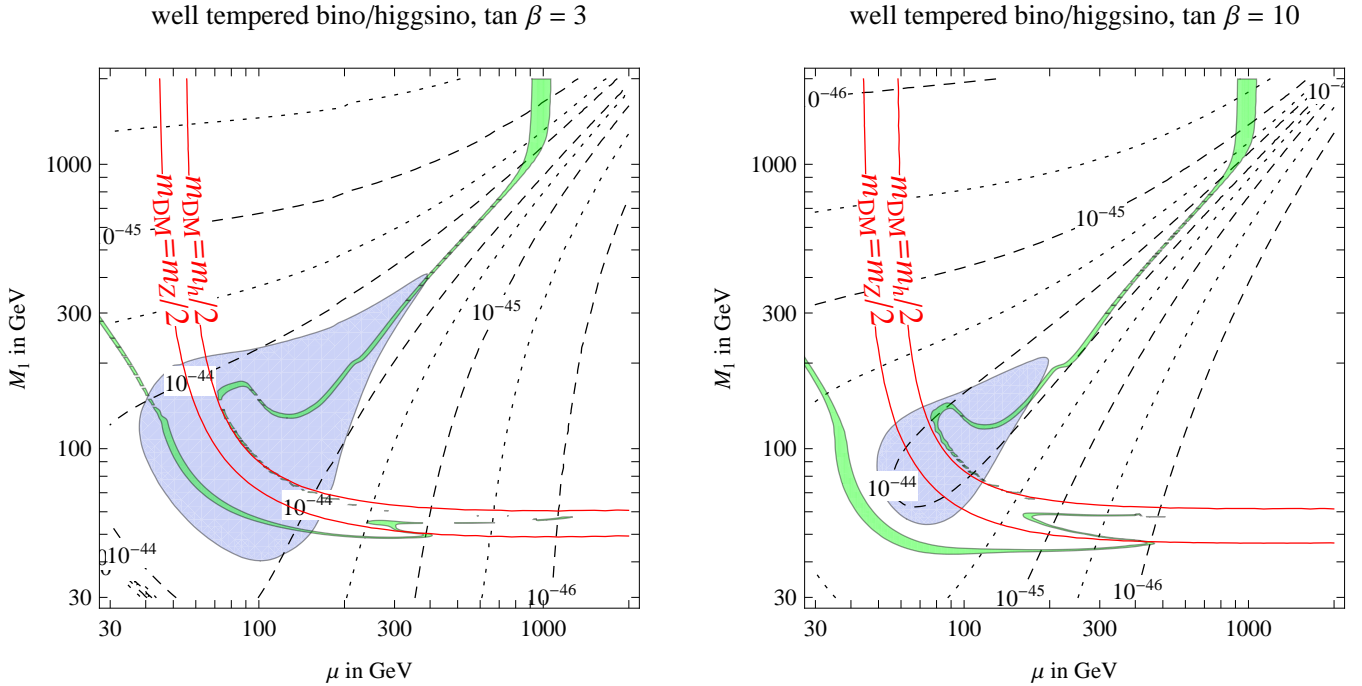


Figure 8: *Model independent “well-tempered” neutralino scenario. The 3σ range for the cosmological DM abundance is reproduced within the green strip. The gray region is excluded by XENON100 [16].*

We thereby focus on a mixed bino/higgsino. In the limit where we can ignore all other heavier sparticles, its phenomenology is fully described by 3 parameters: the bino mass term M_1 , the higgsino mass term μ (we assume them to be positive) and $\tan\beta$. The observed thermal relic DM abundance is reproduced in the green strip in Fig. 8 (left panel for $\tan\beta = 3$ and right panel for $\tan\beta = 10$). The region with $M_1 \approx \mu \approx M_Z$ was allowed, but its large direct detection cross section is now disfavored by XENON100 (gray region). An improvement of the XENON100 bound by a factor of few would fully exclude the whole “well-tempered” neutralino scenario, unless the local DM density or the nuclear matrix element f of eq. (12) are significantly lower than what is assumed in our computation.

The minor tilt at $M_{\text{DM}} \approx m_t$ is due to the top quark threshold. At lower masses, the cosmologically allowed region of Fig. 8 is affected by the Z and Higgs resonances ($2M_{\text{DM}} = M_Z$ or m_h respectively, indicated as red curves). At larger masses, the “well-tempered” neutralino region terminates at $\mu \approx 1$ TeV, where the (almost) pure higgsino becomes a good DM candidate.

5.4 Supersymmetry beyond the CMSSM: pMSSM

In order to relax the theoretical constraints of the CMSSM on the SUSY mass spectrum, we also performed a similar analysis for free low energy SUSY parameters of the MSSM. The low energy phenomenological MSSM, pMSSM, is characterized by the three gaugino masses M_1, M_2, M_3 , the higgsino mass μ , the common squark masses $m_{\tilde{q}}$, the left and right-handed slepton masses $m_{\tilde{L}}, m_{\tilde{E}}$, the Higgs mass parameter m_A and by $\tan\beta$. We randomly scan all these parameters.

Fig. 9 shows our results, in the same notations as the corresponding CMSSM figure, Fig. 4. Because the squark and slepton masses are not related any more via the GUT relations, light

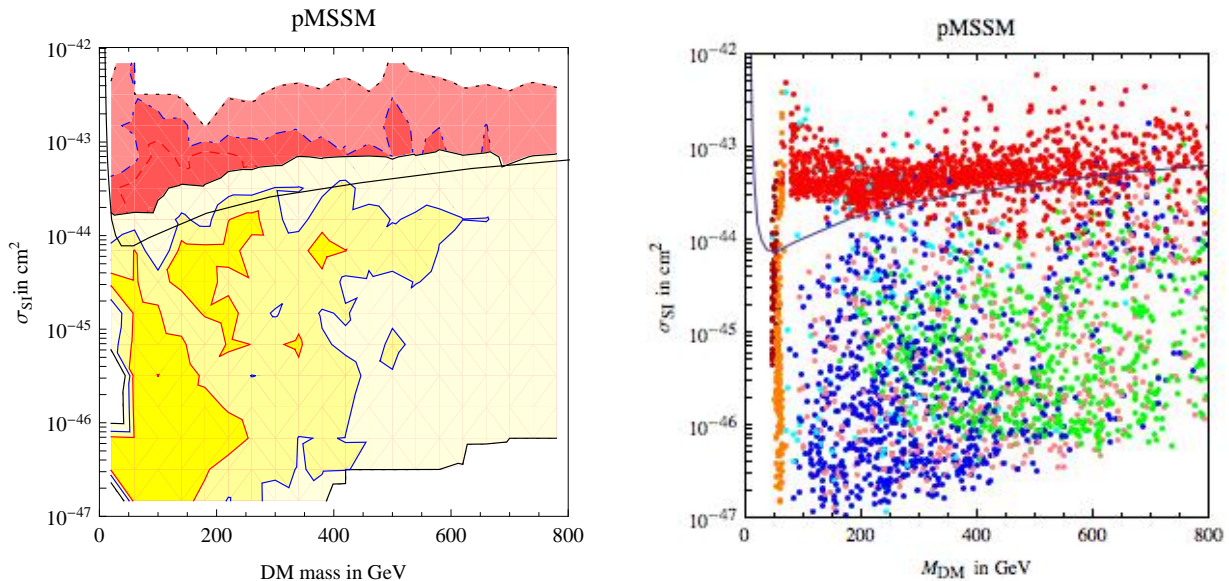


Figure 9: *The pMSSM fit (left panel) in $(M_{\text{DM}}, \sigma_{\text{SI}})$ plane and the corresponding DM generation mechanisms (right panel) in the colour code analogous to Fig. 4 except for two new regions: the pink dots denote “well-tempered” bino/wino and the dark red dots the Z-resonance.*

sleptons become available for a good fit of $(g - 2)_\mu$ that dominates the fit. At the same time, heavy squarks can suppress any new contributions to $b \rightarrow s\gamma$. Therefore a wider range of parameters becomes allowed by the global fit, with still a preference for relatively light DM mass, that again mostly corresponds to neutralino/slepton coannihilations (blue dots in Fig. 9b). Again the region disfavored by the new XENON100 data mostly corresponds to the “well-tempered” bino/higgsino (upper red dots in Fig. 9b). Two new regions appear: “well-tempered” bino/wino (pink dots, at any mass with σ_{SI} below the XENON100 bound), and Z-resonance (dark red dots at $M_{\text{DM}} \gtrsim M_Z/2$). There are now significant overlaps among the various kinds of DM neutralinos and the mechanisms for generating the DM relic abundance are not well separated. Although the pMSSM parameter space is more complicated than the CMSSM one, the results are qualitatively similar.

6 Conclusions

We have performed a fit to the new XENON100 data and, based on that, analyzed several well motivated DM scenarios. We show that XENON100 disfavors the Inelastic Dark Matter interpretation and the light Dark Matter interpretation of the DAMA/LIBRA claim as well as other hints for light DM by CoGeNT and CDMS II.

The first results of the XENON100 experiment exclude part of the parameter space of Dark Matter models coupled to the Higgs boson. The constrained version of the scalar singlet dark matter model (where the DM mass is predicted in terms of DM coupling to the Higgs boson), previously favored by the CDMS hint, gets disfavored. Such model now needs an independent mass term for the scalar singlet around the weak scale, with its associated naturalness problem.

In the context of supersymmetry, we show model independently that the XENON100 data

disfavors the generic scenario of “well-tempered” bino/higgsino proposed as a way to get neutralino DM around the weak scale. Within the CMSSM, the XENON100 data excludes small $|\mu|$, small m_A regions of the parameter space previously allowed in the global fit at 3σ level. As a result the “focus-point” region is ruled out and, most likely, the CMSSM charged Higgs boson mass is not accessible at 7 TeV LHC. The exceptional parameter region with small $M_{1/2}$ that is still allowed at 3σ level is the DM annihilation region via the Higgs boson resonance. That parameter region will be probed by the LHC experiments in 2011 due to the small gluino mass. The remaining CMSSM best fit parameter space at 3σ level is relatively compact in which the DM relic abundance is generated by the slepton co-annihilation processes. Today neither the XENON100 nor the LHC experiments probe the best fit CMSSM parameter space yet but the sensitivity of both experiments will enter into this region.

We obtained qualitatively similar constraints also for the pMSSM. However, the pMSSM parameter space is much larger and cannot be definitely tested by the present experiments.

Note added. After our fits to the new XENON100 data were performed and studies of iDM completed, a similar dedicated study appeared by the XENON Collaboration [56]. Our results agree in that the iDM scattering off sodium is strongly disfavoured as an explanation to the DAMA/LIBRA annual modulation signal. In addition, we also consider iDM scattering off thallium.

Acknowledgements We thank Alexander Pukhov for valuable communication and for providing us with a new version of Micromegas package. This work was supported by the ESF grants 8090, 8499, MTT8 and by SF0690030s09 project. The work of D.P. is supported by the Swiss National Science Foundation under contract No. 200021-116372. The work of M.F. is supported in part by the European Programme “Unification in the LHC Era”, contract PITN-GA-2009-237920 (UNILHC).

References

- [1] D. Larson *et al.*, *Astrophys. J. Suppl.* 192 (2011) 16 [arXiv:1001.4635].
- [2] G. Jungman, M. Kamionkowski and K. Griest, *Phys. Rept.* 267 (1996) 195 [arXiv:hep-ph/9506380].
- [3] J. R. Ellis, J. S. Hagelin, D. V. Nanopoulos, K. A. Olive and M. Srednicki, *Nucl. Phys. B* 238 (1984) 453.
- [4] G. R. Farrar, P. Fayet, *Phys. Lett. B* 76 (1978) 575-579; S. Dimopoulos, H. Georgi, *Nucl. Phys. B* 193 (1981) 150; L. E. Ibanez, G. G. Ross, *Nucl. Phys. B* 368 (1992) 3-37.
- [5] L. M. Krauss, F. Wilczek, *Phys. Rev. Lett.* 62 (1989) 1221.
- [6] M. Kadastik, K. Kannike and M. Raidal, *Phys. Rev. D* 81 (2010) 015002 [arXiv:0903.2475].
- [7] J. Hisano, K. Ishiwata, N. Nagata and T. Takesako, arXiv:1104.0228.
- [8] M. Cirelli, N. Fornengo, A. Strumia, *Nucl. Phys. B* 753 (2006) 178 [arXiv:hep-ph/0512090].
- [9] CDMS-II Collaboration, *Science* 327 (2010) 1619-1621. [arXiv:0912.3592].
- [10] EDELWEISS Collaboration, [arXiv:1103.4070].
- [11] XENON100 Collaboration, arXiv:1103.0303.
- [12] DAMA Collaboration, *Eur. Phys. J. C* 56 (2008) 333 [arXiv:0804.2741].
- [13] CoGeNT collaboration, *Phys. Rev. Lett.* 106 (2011) 131301. [arXiv:1002.4703].
- [14] D. Tucker-Smith and N. Weiner, *Phys. Rev. D* 64 (2001) 043502 [arXiv:hep-ph/0101138].
- [15] S. Chang, G. D. Kribs, D. Tucker-Smith, N. Weiner, *Phys. Rev. D* 79 (2009) 043513 [arXiv:0807.2250].
- [16] E. Aprile *et al.* [XENON100 Collaboration], arXiv:1104.2549 [astro-ph.CO].

- [17] CMS Collaboration, Phys. Lett. B698 (2011) 196 [arXiv:1101.1628].
- [18] ATLAS Collaboration, arXiv:1102.2357; J. B. G. da Costa *et al.* [ATLAS Collaboration], arXiv:1102.5290 [hep-ex].
- [19] N. Arkani-Hamed, A. Delgado, G. Giudice, Nucl. Phys. B741 (2006) 108 [arXiv:hep-ph/0601041].
- [20] J. L. Feng, K. T. Matchev and T. Moroi, Phys. Rev. Lett. **84** (2000) 2322 [arXiv:hep-ph/9908309]; J. L. Feng, K. T. Matchev and T. Moroi, Phys. Rev. D **61** (2000) 075005 [arXiv:hep-ph/9909334].
- [21] M. C. Smith *et al.*, Mon. Not. Roy. Astron. Soc. 379 (2007) 755 [arXiv:astro-ph/0611671].
- [22] R. H. Helm, Phys. Rev. 104, 1466-1475 (1956).
- [23] G. Plante *et al.*, arXiv:1104.2587 [nucl-ex].
- [24] A. Ianni, G. Pagliaroli, A. Strumia, F. R. Torres, F. L. Villante, F. Vissani, Phys. Rev. D80 (2009) 043007 [arXiv:0907.1891].
- [25] S. Chang, R. F. Lang and N. Weiner, Phys. Rev. Lett 206 (2011) 011301 [arXiv:1007.2688].
- [26] J. McDonald, Phys. Rev. D50 (1994) 3637.
- [27] C. Burgess, M. Pospelov, T. ter Veldhuis, arXiv:hep-ph/0011335
- [28] V. Barger, P. Langacker, M. McCaskey, M. Ramsey-Musolf, G. Shaughnessy, Phys. Rev. D77 (2008) 035005 [arXiv:0706.4311].
- [29] X. He, T. Li, X. Li, J. Tandean, H. Tsai, arXiv:0912.4722.
- [30] M. Farina, D. Pappadopulo, A. Strumia, Phys. Lett. B688 (2010) 329 [arXiv:0912.5038].
- [31] L.L. Honorez and C.E. Yaguna, JHEP 046 (2010) 1009 [arXiv:1003.3125].
- [32] P. Salucci, F. Nesti, G. Gentile and C. F. Martins, arXiv:1003.3101.
- [33] J. Ellis, K.A. Olive, C. Savage, arXiv:0801.3656.
- [34] J. Giedt, A.W. Thomas, R.D. Young, arXiv:0907.4177.
- [35] G. Belanger, F. Boudjema, A. Pukhov, A. Semenov, Comput. Phys. Commun. 176 (2007) 367-382 [hep-ph/0607059]; G. Belanger, F. Boudjema, A. Pukhov, A. Semenov, Comput. Phys. Commun. 149 (2002) 103-120 [hep-ph/0112278]; G. Blanger, F. Boudjema, P. Brun, A. Pukhov, S. Rosier-Lees, P. Salati, A. Semenov, Comput. Phys. Commun. 182 (2011) 842 [arXiv:1004.1092].
- [36] D. Feldman, K. Freese, P. Nath, B. D. Nelson and G. Peim, arXiv:1102.2548.
- [37] B. C. Allanach, arXiv:1102.3149.
- [38] O. Buchmueller *et al.*, arXiv:1102.4585.
- [39] P. Bechtle *et al.*, arXiv:1102.4693.
- [40] S. Akula, N. Chen, D. Feldman, M. Liu, Z. Liu, P. Nath and G. Peim, arXiv:1103.1197.
- [41] J. A. Conley, J. S. Gainer, J. L. Hewett, M. P. Le and T. G. Rizzo, arXiv:1103.1697.
- [42] S. Akula, D. Feldman, Z. Liu, P. Nath and G. Peim, arXiv:1103.5061.
- [43] S. Bethke, Eur. Phys. J. C64 (2009) 689 [arXiv:0908.1135].
- [44] CDF Mtop combination, Fabrizio Margaroli, "Top quark properties at the Tevatron On behalf of CDF and D0 collaboration," Moriond EW2011.
- [45] K. Nakamura *et al.* [Particle Data Group], J. Phys. G 37 (2010) 075021.
- [46] D. Larson *et al.*, Astrophys. J. Suppl. 192 (2011) 16 [arXiv:1001.4635].
- [47] M. Davier, A. Hoecker, B. Malaescu, Z. Zhang, Eur. Phys. J. C71 (2011) 1515. [arXiv:1010.4180].
- [48] M. Misiak *et al.*, Phys.Rev.Lett. 98 (2007) 022002 [arXiv:hep-ph/0609232]. For a recent update see M. Misiak, arXiv:1010.4896.

- [49] LHCb collaboration, arXiv:[1103.2465](#). D0 collaboration, arXiv:[1006.3469](#). CDF collaboration, talk by J. Parsons at BLOIS'10 17/7/2010.
- [50] O. Buchmueller, R. Cavanaugh, A. De Roeck, J. R. Ellis, H. Flacher, S. Heinemeyer, G. Isidori, K. A. Olive *et al.*, Eur. Phys. J. C64 (2009) 391-415. [arXiv:[0907.5568](#)].
- [51] G. Marandella, C. Schappacher, A. Strumia, Nucl. Phys. B715 (2005) 173 [arXiv:[hep-ph/0502095](#)].
- [52] A. Strumia, arXiv:[1101.2195](#).
- [53] S. Cassel, D. M. Ghilencea, S. Kraml, A. Lessa and G. G. Ross, arXiv:[1101.4664](#).
- [54] O. Buchmueller *et al.*, Eur. Phys. J. C 71 (2011) 1583 [arXiv:[1011.6118](#)].
- [55] J. Hisano, S. Matsumoto, O. Saito, M. Senami, Phys. Rev. D73 (2006) 055004 [arXiv:[hep-ph/0511118](#)]. M. Cirelli, A. Strumia and M. Tamburini, Nucl. Phys. B787 (2007) 152 [arXiv:[0706.4071](#)].
- [56] E. Aprile *et al.*, [XENON100 Collaboration], arXiv:[1104.3121](#).